

Enhanced distance regularization for re-initialization free level set evolution with application to image segmentation

Xuchu Wang ^{a,*}, Jinxiao Shan ^a, Yanmin Niu ^b, Liwen Tan ^c, Shao-Xiang Zhang ^c

^a Key Laboratory of Optoelectronic Technology and Systems of Ministry of Education, College of Optoelectronic Engineering, Chongqing University, Chongqing 400044, PR China

^b College of Computer and Information Science, Chongqing Normal University, Chongqing 400050, PR China

^c Department of Anatomy, Third Military Medical University, Chongqing 400038, PR China

ARTICLE INFO

Article history:

Received 1 April 2013

Received in revised form

6 March 2014

Accepted 9 March 2014

Communicated by D. Tao

Available online 13 April 2014

Keywords:

Level set evolution

Re-initialization free method

Distance regularization

Forward and backward diffusion

Active contours

Image segmentation

ABSTRACT

In level set methods, the re-initialization remedy is widely applied to periodically replace the degraded level set function (LSF) with a signed distance function to maintain its regularity. Due to its various limitation, the energy functional regularization based methods using variational technique (e.g. distance, Gaussian, and reaction-diffusion based regularization methods) are recently introduced to replace this remedy. However, the relationship among them seems to be less investigated. In this paper, an enhanced distance regularized level set evolution (DRLSE-E) completely free of the re-initialization procedure is proposed based on analyzing these recent regularization models. DRLSE-E has an intrinsic capability of maintaining LSF's regularity, particularly the desirable signed distance property in a vicinity of the zero level set and the flat property out of this vicinity, which ensures accurate computation and stable level set evolution. Like other re-initialization free methods, DRLSE-E has simple and efficient numerical scheme in implementation, flexible initialization. Furthermore, DRLSE-E has the advantage of faster evolving speed and more numerical accuracy than distance regularized methods because of its forward and backward diffusion rate considering two competing components during the evolution. As an application example, DRLSE-E is used to typical edge-based and region-based active contour models for image segmentation and shows its competitiveness. Considering DRLSE-E is general, it can be easily incorporated into various existing level set models for image segmentation, filtering, and other tasks.

© 2014 Elsevier B.V. All rights reserved.

1. Introduction

In the last 20 years, active contour models (ACMs, snakes or deformable models) [1,2] have received extensive attention in the fields of image processing and computer vision, especially for image segmentation [3–5]. These methods all need to initialize a closed curve in the image and then evolve it until the evolving curve converges to the target [6,7]. According to the representation of the evolving curve, ACM can be roughly divided into parametric ACM [1,8] and geometric ACM [9]. The parametric ACM uses parametric equation to explicitly represent the evolving curve. The explicit representation easily brings some intrinsic drawbacks, such as difficulty in handling topological changes, limitation in capture range of concave boundaries, and dependency of parameterizations.

On the contrary, the geometric ACM implicitly represents the curves as the zero level set (LS) of a higher dimensional function,

called LS function (LSF), and formulates the evolution of the curves through the evolution of LSF. The curve is evolved using the partial differential equation (PDE) derived from the energy function that describes a curve smoothing process. When the curve evolution stops, the zero LS corresponds to the segmentation result. The geometric ACM using the LS evolution (LSE) can naturally represent contour of complex topology and deal with topological changes (contour breaking and merging) without any extra functions by controlling the evolution of LSF rather than the parametric curves. Thus it significantly improves ACM by being free of the drawbacks in parametric ACM. Moreover, extensive numerical algorithms based on Hamilton–Jacobi equations have been developed, accurately handling shocks and providing stable numerical schemas [9,10]. These merits make LS methods a popular numerical technique for tracking moving interfaces or segmenting objects in image processing, computer vision, computer graphics, computational geometry, fluid mechanics, material sciences, etc. [11–15].

In LS evolution methods for image segmentation, the LSF is commonly defined by computing the closest distances between pixels and a given closed curve in an image domain. To obtain a clear zero LS as the boundary, the points that have positive

* Corresponding author. Tel.: +86 23 65102516; fax: +86 23 65102515.

E-mail addresses: seadrift.wang@gmail.com (X. Wang), niuym@cqnu.edu.cn (Y. Niu).

distances are inside the curve, and ones that have negative distances are outside the curve. Although the initial front would work for any function negative inside and positive outside, the signed distance function (SDF) gives many desirable properties [16]. Specifically, the SDF ϕ in a metric space (\mathbf{X}, d) is defined by

$$\phi = \begin{cases} -d(\mathbf{x}, \partial S) & \text{if } \mathbf{x} \in S^- \\ 0 & \text{if } \mathbf{x} \in \partial S \\ d(\mathbf{x}, \partial S) & \text{if } \mathbf{x} \in S^+ \end{cases} \quad (1)$$

where $d(\mathbf{x}, S) = \inf_{\mathbf{y} \in S} d(\mathbf{x}, \mathbf{y})$ denotes the distance of a given point \mathbf{x} to the boundary of S . If $S \subseteq \mathbb{R}^n$ with piecewise smooth boundary, the SDF is differentiable almost everywhere, and its gradient satisfies the Eikonal equation $|\nabla \phi| = 1$. This property close relates to the unit normal vector, the mean curvature, the closest point on the boundary, and the simplified volume and surface integrals on the domain. Therefore, the LSF is usually forced to be a SDF, especially in the evolving stage. However, during the iterative cycles of evolution, the size of the gradient of the SDF may become too small at certain points, that is, the property of SDF does not hold, which may cause numerical instabilities and even errors during computation. It is necessary to re-initialize the LS function as a SDF again to remedy this degeneracy or irregularities. In conventional LS methods, re-initialization is performed by periodically stopping the evolution and reshaping the degraded LSF as a SDF [17–19,10]. However, the use of re-initialization introduces some fundamental problems yet to be practically solved, such as no general answers to when and how to apply the re-initialization [20,21]. Re-initialization is often applied in an ad hoc manner, and it should be avoided as much as possible [18,22].

To reduce or eliminate the re-initialization step, the global minimization methods [23,24] are introduced to incorporate into some variational LSF via the specific form based total variation approach, such as Chan–Vese model [25] and Vese–Chan's piecewise smoothing model [26]. The convex object function in these methods is helpful for keeping the LSF's regularity during the evolution. From another aspect, the constrained diffusion-based LSE [27] is proposed to deal with the initialization dependency problem that commonly appears in edge-based approaches. The diffusion rate in this method changes smoothly from 0 to 1 and makes LSF tend to flat. By extending the radial basis functions (RBF) based LSE, a region based ACM not requiring any initialization [28,29] is further proposed. In this method, the LSF is interpolated using RBFs. Its shape and topology are determined by the coefficients of RBF interpolation. So, the finite difference based numerical methods to evolve the LSF are replaced by the adaptive changes of the RBF interpolation coefficients. The regularization of LSF is intrinsically handled through velocity normalization and the smoothing nature of RBF interpolation, and the periodic re-conditioning can be eliminated via RBF coefficient updating. Besides these methods, an efficient non-convex minimization algorithm [30] is proposed for distance preserving LS methods. This method overcomes the main numerical limitations by introducing constrained L_1 optimization techniques via splitting this non-convex problem into sub-optimizations, and then combining them together using an augmented Lagrangian approach [31].

Recently, the variational LSE is introduced to eliminate the costly re-initialization procedure by incorporating a penalty term into the energy functional [32]. This method has received significant attentions because it repairs the critical but bottleneck-like disagreement between theory and implementation in LSE. Unfortunately, this penalty term may cause an undesirable side effect on the LSF in some circumstances, which may affect the numerical accuracy. To address this, an improved variational LS formulation [22] is further developed by incorporating a distance regularization term into the energy functional, and completely avoiding the undesirable side effect arisen from the penalty term.

It is theoretically graceful and practically advisable for the investigation on a new double-well potential related to the distance regularization term to maintain a desired shape of the LSF.

Besides this, a Gaussian filter is recently proposed to regularize the LSF to achieve local segmentation and did not employ the re-initialization in numerical implementation [33]. In this method, the evolution of a function with its Laplacian derivation is equivalent to Gaussian filtering the initial condition of the function, so this method can be called as Gaussian regularized LS evolution (GRLSE). This regularization approach has received remarkable attentions because it is very fast, exact in segmenting clean objects, efficient in numerical implementation, and capable of adaptively selecting local or global segmentation. However, the energy functional in the penalty term is not explicitly presented, and the stability of the curves under the proposed LS formulation is not thoroughly investigated. More recently, a novel reaction-diffusion (RD) method [34] for implicit active contours is further presented, which is free of the costly re-initialization. The RD equation in phase transition modeling is based on the Van der Waals–Cahn–Hilliard theory in mechanics for stability analysis of systems with unstable components, and the RD term is introduced into penalty to derive a piecewise constant solution. Accordingly, this method performs well on weak boundary anti-leakage and noisy image. However, this method evolves slower than GRLSE.

We focus our topic on the regularization based variational LSE free of re-initialization. Although the four methods are advisable in image segmentation applications, there are some interesting questions among them. First, what is the intrinsic relationship among the distance regularized methods and the Gaussian regularized ones? Since they all are proposed independently in recent years, it seems that their relationship and their characteristic are less investigated. Second, in experiments it is found that the GRLSE method performs well for less iteration number but when the iteration number increases, it cannot segment the object anymore, what is reason for this? Third, the forward and backward diffusion is interesting in distance regularized methods, can the diffusion rate be further improved?

Motivated by these questions, in this paper, we proposed a new variational LSE, namely DRLSE-E, with an enhanced distance regularization energy term that drives the motion of the zero level contours toward desired locations. In our method, to maintain a desired shape of the LSF, particularly the desirable signed distance property in a vicinity of the zero LS and the flat property out at this vicinity, a new distance regularization term is defined to force the gradient magnitude of the LSF to one of its minimum points. It ensures accurate computation and stable LS evolution. The LSE is derived as a gradient flow that minimizes a double-well energy functional for the distance regularization term, which derives a forward-and-backward diffusion to maintain the regularity of LSF. Besides re-initialization-free property, the internal energy functional of DRLSE-E explicitly emphasizes the competition of signed distance preserving component and flat component for small gradient magnitude, while accelerates the gradient descent velocity for large gradient magnitude in different LSs, which makes DRLSE-E very simple and fast in numerical implementation. To validate DRLSE-E, we apply it to edge-based and region-based ACM for image segmentation, and compared them to some related methods. The experimental results on synthetic and real-world images demonstrate the advantage of DRLSE-E, e.g., implementation with a simpler and more efficient numerical scheme than conventional LSE, and relatively large time steps and computation time, while ensuring competitive numerical accuracy and efficiency.

The rest of this paper is organized as follows. In Section 2, we introduce some related works. In Section 3, we propose a new variational LSE with an enhanced distance regularization term.

In [Section 4](#), we apply the proposed formulation to typical edge-based and region-based model for image segmentation. Experimental results are reported in [Section 5](#) and we summarize our work in [Section 6](#).

2. Related works

2.1. Distance regularized LSE

Li et al. [32] proposed a re-initialization-free distance regularized LS evolution method (DRLSE1). This method defines an intrinsic energy functional as

$$\mathcal{R}_{P_1}(\phi) = \int_{\Omega} P_1(|\nabla\phi|) d\mathbf{x} \quad (2)$$

on the image domain Ω , and

$$P_1(|\nabla\phi|) = \frac{1}{2}(|\nabla\phi| - 1)^2 \quad (3)$$

is defined to penalize the deviation of the LSF from a signed distance function (SDF). Minimizing the above energy functional by using the steepest descent method, and representing the contour C with zero LS, i.e. $\phi(\mathbf{x}) = 0$, the following variational formulation is obtained:

$$\frac{\partial\phi}{\partial t} = \Delta\phi - \operatorname{div}\left(\frac{\Delta\phi}{|\nabla\phi|}\right) = \operatorname{div}\left\{\left(1 - \frac{1}{|\nabla\phi|}\right)\nabla\phi\right\}. \quad (4)$$

[Eq. \(4\)](#) is a typical heat diffusion equation with diffusion rate $r = 1 - 1/|\nabla\phi|$. If $|\nabla\phi| > 1$, $r > 0$, the forward diffusion will decrease $|\nabla\phi|$. If $|\nabla\phi| < 1$, the corresponding backward diffusion will increase $|\nabla\phi|$. As a result, the final diffusion result tends to make and the character of SDF is preserved, i.e. $|\nabla\phi| = 1$, and the energy functional achieves its minimum. This penalty functional provides a mechanism of maintaining the signed distance property of LSF, and the need for re-initialization can be eliminated. Furthermore, it allows the use of a simpler and more efficient numerical scheme in the implementation than those used for conventional LS formulations. However, this penalty term may cause an undesirable side effect on LSF in some circumstances, which may affect the numerical accuracy, since the purpose of imposing the LS regularization term is not only to smooth the LSF, but also to maintain the signed distance property for accurate computation in curve evolution, at least in a vicinity of the zero LS.

To overcome the side effect, Li et al. [22] further proposed an improved distance regularized LS evolution method (DRLSE2) with a new penalty term as

$$P_2(|\nabla\phi|) = \begin{cases} \frac{1}{2}(|\nabla\phi| - 1)^2; & |\nabla\phi| \geq 1 \\ \frac{1}{(2\pi)^2}(1 - \cos(2\pi|\nabla\phi|)); & |\nabla\phi| \leq 1 \end{cases} \quad (5)$$

Note that $|\nabla\phi| = 1$ is rewritten to emphasize this region. DRLSE2 is characterized in the double-well of the penalty term that results in two global minimum points $|\nabla\phi| = 0$ and $|\nabla\phi| = 1$. In calculus of variations, a standard method to minimize $P_2(|\nabla\phi|)$ is to find the steady state solution of the gradient flow equation. Then the resulting PDE is still a heat diffusion equation

$$\frac{\partial\phi}{\partial t} = \begin{cases} \operatorname{div}\left((1 - \frac{1}{|\nabla\phi|})\nabla\phi\right); & |\nabla\phi| \geq 1 \\ \operatorname{div}(\operatorname{sinc}(2|\nabla\phi|)\nabla\phi); & |\nabla\phi| \leq 1 \end{cases} \quad (6)$$

with diffusion rate

$$r = \begin{cases} 1 - \frac{1}{|\nabla\phi|}; & |\nabla\phi| \geq 1 \\ \operatorname{sinc}(2|\nabla\phi|); & |\nabla\phi| \leq 1 \end{cases} \quad (7)$$

where $\operatorname{sinc}(x) = \sin(2\pi x)/2\pi x$. Apparently,

$$\lim_{|\nabla\phi| \rightarrow 0} r = \lim_{|\nabla\phi| \rightarrow \infty} r = 1, \quad (8)$$

which verifies the stableness and bound of the diffusion rate. Therefore, the evolution by [Eq. \(5\)](#) decreases the fluctuation in [Eq. \(3\)](#). The character of SDF is preserved in the vicinity of zero LS region, meanwhile, the fluctuations are reduced far away from this region.

2.2. Gaussian regularized LSE

Zhang et al. [33] recently proposed a Gaussian regularized LS evolution method (GRLSE) to avoid the complexity of evolution of traditional LS. GRLSE reformulates the LS evolution equation as

$$\frac{\partial\phi}{\partial t} = \beta|\nabla\phi|, \quad (9)$$

where $|\nabla\phi|$ is the magnitude of normal of the curve. To obtain a smooth curve, GRLSE settles β as the average curvature, then [Eq. \(9\)](#) can be rewritten as

$$\frac{\partial\phi}{\partial t} = \operatorname{div}\left(\frac{\nabla\phi}{|\nabla\phi|}\right)|\nabla\phi|. \quad (10)$$

GRLSE further considers the property of SDF, i.e. $|\nabla\phi| = 1$, to simplify the LSF, so

$$\frac{\partial\phi}{\partial t} = \operatorname{div}(\nabla\phi) = \Delta\phi, \quad (11)$$

where Δ is the Laplacian operator. The solution for this isotropic heat diffusion equation is the initial value of ϕ convolved with Gaussian function with different kernel. It means

$$\phi_t = G_t * \phi_0, \quad (12)$$

where ϕ_0 is the initial value of LSF and ϕ_t is the value of LSF at time t , and G_t is the Gaussian kernel at scale t . Thus, the evolution of GRLSE can be represented as

$$\phi_{t+\Delta t}^{n+1} = G_{\Delta t} * \phi_t^n. \quad (13)$$

By this way, the procedure of periodical re-initialization in traditional LSE can be eliminated. This strategy makes GRLSE fast. However, the energy functional in GRLSE is not explicitly expressed, which increases the analytical difficulty of this method.

2.3. Reaction diffusion based LSE method

Zhang et al. [34] recently further proposed a re-initialization-free LSE by constructing a reaction-diffusion (RD) equation. In their method, a diffusion term is added into the conventional LSE equation $\partial\phi/\partial t = -F|\nabla(\phi)|$ or $\partial\phi/\partial t = F\delta(\phi)$ under the initial condition $\phi(\mathbf{x}, t=0) = \phi_0(\mathbf{x})$, where F is a velocity parameter. Specifically, the RD equation for the LSE is

$$\frac{\partial\phi}{\partial t} = \varepsilon\Delta\phi - \frac{1}{\varepsilon}L(\phi) \quad (14)$$

with initial condition $\phi(\mathbf{x}, t=0, \varepsilon) = \phi_0(\mathbf{x})$, where $L(\phi) = -F|\nabla(\phi)|$ for PDE based LSE or $L(\phi) = -F\delta(\phi)$ for variational LSE, Δ is a Laplacian operator and ε is a small positive constant. The diffusion term $\varepsilon\Delta\phi$ and the reaction term $-(1/\varepsilon)L(\phi)$ in [Eq. \(14\)](#) jointly perform the dynamic process to determine the evolving interface of the LS [35]. The Van der Waals–Cahn–Hilliard theory ensures the uniqueness of the solution by introducing a simple singular perturbation with a very small constant [36].

In their viewpoints, the diffusion term emancipates the conventional LSE from the extra re-initialization procedure by regularizing the LSF. This opinion is quite informative for investigating the shape of the LS. The RD method is implemented by two-step

splitting technique, where the first step is the numerical iteration to obtain the viscosity solution of the equation $\partial\phi/\partial t = -(1/\varepsilon)L(\phi)$, and the second step is the isotropic heat diffusion according to equation $\partial\phi/\partial t = \varepsilon\Delta\phi$ on this viscosity solution. The whole time step is combined by the time steps corresponding to each iteration. Since there exists the competition between these two evolutions, the time step for each evolution needs fine consideration to satisfy the Von Neumann boundary condition [37]. Thus, the time consumption increases due to this competition characteristic in numerical implementation.

3. Enhanced DRLSE

3.1. Analysis on the regularization based LSE and our motivation

The recent regularization based LSE methods (such as DRLSE1, DRLSE2, GRLSE, and RD) all avoid the problem of re-initialization in traditional LSE, however, their computational efficiency, energy functional and zero LS are quite different. This claim is supported by the following analysis in the viewpoint of the gradient magnitude of the LS.

- (1) The SDF penalty in DRLSE1 greatly improves the numerical efficiency of PDE for avoiding the re-initialization procedure. However, when $|\nabla\phi| \rightarrow 0$, the diffusion $r \rightarrow -\infty$ and Eq. (3) will diffuse backwards with an arbitrary diffusion rate, then $|\nabla\phi|$ will increase rapidly, along with the instability of diffusion, and the final LS function will fluctuate rapidly. Although this fluctuation does not appear in the zero LS, the localization of zero LS will be disturbed. As a refinement, DRLSE2 avoids the fluctuations of LS evolution and emphasizes the smoothness of LS function. However, due to the character of the potential (or energy density) function, it needs more iteration to obtain the desirable results.
- (2) As another way, GRLSE obtains the isotropic heat diffusion equation to build the LSE equation by the assumption of $|\nabla\phi| = 1$. It avoids the step of re-initialization in traditional LSE methods and remarkably improves the evolution efficiency. However, it does not explicitly express the energy functional that is essential for analysis the evolution process. It also should be noticed that the condition $|\nabla\phi| = 1$ is not absolutely satisfactory in numerical implementation. Furthermore, we propose the following proposition about this method.

Proposition 1. *The zero LS will disappear along with the unstable evolution in the GRLSE method [33].*

Proof. Define an energy functional as

$$\mathcal{R}_{P_3}(\phi) = \frac{1}{2} \int_{\Omega} |\nabla\phi|^2 d\mathbf{x} \quad (15)$$

with a penalty term

$$P_3(|\nabla\phi|) = |\nabla\phi|^2/2, \quad (16)$$

it is obvious that when $|\nabla\phi| = 0$ the minimum of $\mathcal{R}_{P_3}(\phi)$ is 0. In calculus of variations, a standard method to minimize $\mathcal{R}_{P_3}(\phi)$ is to find the steady state solution of the gradient flow equation

$$\frac{\partial\phi}{\partial t} = -\frac{\partial\mathcal{R}_{P_3}(\phi)}{\partial\phi}, \quad (17)$$

where $\partial\mathcal{R}_{P_3}/\partial\phi$ is the Gâteaux derivative of $\mathcal{R}_{P_3}(\phi)$ with respect to ϕ . Then the resulting PDE is

$$\frac{\partial\phi}{\partial t} = |\nabla\phi| \operatorname{div} \left(\frac{\nabla\phi}{|\nabla\phi|} \right) = \operatorname{div}(\nabla\phi) = \Delta\phi. \quad (18)$$

The same isotropic diffusion equation is obtained with respect to Eq. (11). Therefore, to reach the minimum of $\mathcal{R}_{P_3}(\phi)$, $|\nabla\phi| \rightarrow 0$, the zero LS will disappear along with the iteration proceeds. \square

As a result, Eq. (15) is the energy functional of GRLSE method. In other words, GRLSE emphasizes the character of $|\nabla\phi| \rightarrow 0$, while discards the key characteristic of $|\nabla\phi| = 1$. It is noticed that the proof does not use the definition of mean curvature. This processing is similar to the Gaussian filtering-based image smoothing that will eventually output a constant image. Although this claim is somewhat unexpected for the eventually evolving result, it still can capture the object to be segmented fast in case that an appropriate number of iteration is chosen or the degenerated LSF is modified properly [33]. Furthermore, it is also close to the total variation-based regularization method that smoothes the LSF [38].

The RD model eliminates the re-initialization procedure according to phase transition modeling based on the Van der Waals–Cahn–Hilliard theory in mechanics for stability analysis of systems with unstable components [36]. Similar to the reaction-diffusion equation in [35] and our proposition on GRLSE, the diffusion term $\varepsilon\Delta\phi$ that gradually regularizes the LSF to be piecewise constant in each segment domain and the reaction term $-(1/\varepsilon)L(\phi)$ that forces the final stable solution to $L(\phi) = 0$. In a word, the RD model uses the isotropic diffusion function to regularize the LSF generated by the Hamilton–Jacobi (H–J) reaction function [9,10].

To ensure the uniqueness of the solution, the ε should be settled as a very small constant to play a switch role satisfying the conservation law in Burgers equation [39]. This reduces the zero LS of LSF from the disappearance while increases the computation burden of the H–J equation. Therefore, the second step in RD model still plays a regularization role, similar to that in GRLSE model except that RD use the iteration approach while GRLSE use the convolution approach under different time steps. Furthermore, they both can be regarded as a distance regularization to keep the flat property of the LSF, e.g. $|\nabla\phi| = 0$, during the forward diffusion, while in DRLSE2 the diffusion is forward and backward together to keep the different properties of the LSF, e.g. $|\nabla\phi| = 1$ or $|\nabla\phi| = 0$ in different regions. Thus, in order to combine the merits of DRLSE, GRLSE, and RD with higher computational stableness and efficiency, it is necessary to explore new energy functional in variational re-initialization-free LSE.

3.2. Proposed energy functional and LS solution

In DRLSE based methods, the initial LS function is usually represented as

$$\phi_0(x) = \begin{cases} -c_0; & x \in \Omega_0 - \partial\Omega_0 \\ 0; & x \in \partial\Omega_0 \\ c_0; & x \in \Omega - \Omega_0 \end{cases} \quad (19)$$

where Ω denotes the image domain, Ω_0 the inner region of contour, $\partial\Omega_0$ the contour of Ω_0 . It is obvious that the magnitude of the LS $|\nabla\phi|$ is large in the region near to $\partial\Omega_0$, while small (even approximately to zero) in the region far from $\partial\Omega_0$. We can view the evolution process of the LS function as the smoothing process of $|\nabla\phi|$ on the image with some constraints of $|\nabla\phi| = 0$ and $|\nabla\phi| = 1$ in different regions. Theoretically, the final localization of contour will be accurate if the characteristic of SDF is preserved better. In other words, the accurate result can be achieved through less iterations if the characteristic of SDF is preserved as much as possible. To this end, we propose an enhanced distance regularized LS evolution method (DRLSE-E) to maintain the properties of the LSF, and thereby avoiding the costly re-initialization step. DRLSE-E achieves this goal by defining an internal energy

functional as

$$\mathcal{R}_P(\phi) = \int_{\Omega} P(|\nabla\phi|) d\mathbf{x}, \quad (20)$$

with a new penalty term defined by

$$P(|\nabla\phi|) = \begin{cases} \frac{1}{2}(|\nabla\phi|^2 - 1) - \ln|\nabla\phi|; & |\nabla\phi| \geq 1 \\ \frac{1}{2}(|\nabla\phi|(|\nabla\phi| - 1))^2; & |\nabla\phi| \leq 1 \end{cases} \quad (21)$$

Apparently, $|\nabla\phi| = 1$ or $|\nabla\phi| = 0$ (corresponding to the signed distance property in the vicinity of the zero LS, and the flat property in other regions) will make $\mathcal{R}_P(\phi)$ reach its minimums. $P(|\nabla\phi|)$ tends to express this via treating two competing components $|\nabla\phi| - 0$ and $|\nabla\phi| - 1$ equally in the region where $|\nabla\phi| \leq 1$ and forcing $|\nabla\phi|$ to be 1 with an accelerator in other regions. This approach remarkably differs from the penalty term in DRLSE1 or DRLSE2 model, where the \cos function seems less reflecting the competition on the two minimum points in driving the LSF.

In calculus of variations, denoting $\partial\mathcal{R}_P/\partial\phi$ as the Gâteaux derivative of the functional \mathcal{R}_P , the standard method to minimize $\mathcal{R}_P(\phi)$ is to find the steady state solution of the gradient flow equation $\partial\phi/\partial t = -\partial\mathcal{R}_P/\partial\phi$, and representing the contour C with zero LS, i.e. $\phi(\mathbf{x}) = 0$ with initial condition $\phi(\mathbf{x}, 0) = \phi_0(\mathbf{x})$, the solution corresponds to the steady state of the following PDE:

$$\frac{\partial\phi}{\partial t} = \begin{cases} \operatorname{div}\left(\left(1 - \frac{1}{|\nabla\phi|^2}\right)\nabla\phi\right); & |\nabla\phi| \geq 1 \\ \operatorname{div}((2|\nabla\phi| - 1)(|\nabla\phi| - 1)\nabla\phi); & |\nabla\phi| \leq 1 \end{cases} \quad (22)$$

This is a heat diffusion equation with diffusion rate

$$r(|\nabla\phi|) = \begin{cases} 1 - \frac{1}{|\nabla\phi|^2}; & |\nabla\phi| \geq 1 \\ (2|\nabla\phi| - 1)(|\nabla\phi| - 1); & |\nabla\phi| \leq 1 \end{cases} \quad (23)$$

and

$$\lim_{|\nabla\phi| \rightarrow 0} r = \lim_{|\nabla\phi| \rightarrow \infty} r = 1. \quad (24)$$

This stable boundary condition verifies the bound of the diffusion rate. It can be found from Eq. (23): (1) for $|\nabla\phi| > 1$, $r > 0$, the diffusion in Eq. (22) is forward, which decreases $|\nabla\phi|$ to 1; (2) for $1/2 < |\nabla\phi| < 1$, $r < 0$, the diffusion in Eq. (22) is backward, which increases $|\nabla\phi|$ to 1; (3) for $|\nabla\phi| < 1/2$, $r > 0$, the diffusion in Eq. (22) is forward, which decreases $|\nabla\phi|$ to 0. Such diffusion is called a forward-and-backward (FAB) diffusion [40,41]. This FAB diffusion drives $|\nabla\phi|$ to be close to one of the minimum points corresponding to the minimum of $\mathcal{R}_P(\phi)$ through adaptively increasing or decreasing $|\nabla\phi|$, thereby maintaining the desired shape of the LSF. Eventually, the evolution makes $|\nabla\phi| = 1$ in the

region nearby zero LS while $|\nabla\phi| = 0$ far away from this region, thus the costly re-initialization step is avoided.

The diffusion rate in DRLSE-E is a piecewise function that controls the similar but more reasonable diffusion behavior in comparison to that in DRLSE2. As plotted in Fig. 1, suppose r_1, r_2 are the diffusion rates of DRLSE2 and DRLSE-E respectively, DRLSE-E can improve the ability of maintaining the desired property of the LSF by:

- (1) For $|\nabla\phi| > 1$, $r_2 > r_1 > 0$, DRLSE-E smoothes $|\nabla\phi|$ heavily in comparison to DRLSE1 and DRLSE2, thus makes $|\nabla\phi| \rightarrow 1$ using less number of iterations.
- (2) For $1/2 < |\nabla\phi| < 1$, both DRLSE2 and DRLSE-E are with background diffusion, the diffusion rate of DRLSE-E is greater than that of DRLSE2 due to $r_1 < r_2 < 0$. In fact the gratitude is larger in the region near to zero LS than other regions. The diffusion of gratitude can be viewed as a process of collapse toward other regions. There must be a process of $|\nabla\phi|$ from $|\nabla\phi| < 1/2$ to $1/2 < |\nabla\phi| < 1$ in a close region approach to the zero LS. This procedure makes the diffusion in this region backward. Thus, there are two types of diffusion in a total diffusion, where the backward diffusion suppresses the forward diffusion. The smaller the backward diffusion is, the larger it suppresses the forward diffusion. Therefore, the constraint of backward diffusion on the forward diffusion in DRLSE-E is less than DRLSE2.
- (3) For $|\nabla\phi| < 1/2$, both DRLSE and DRLSE-E are with forward diffusions, the results make $|\nabla\phi| = 0$. Due to the region with $|\nabla\phi| < 1/2$ is far away from zero LS, the diffusion in the region less affects the forward diffusion.

Therefore, the DRLSE-E outperforms the DRLSE in two facts: (1) its internal energy functional explicitly introduces two competing components $|\nabla\phi| - 0$ and $|\nabla\phi| - 1$ when $|\nabla\phi| \leq 1$, while accelerates the gradient descent velocity by introducing a component $\ln|\nabla\phi|$ for $|\nabla\phi| \geq 1$; (2) it avoids the computation of sinc function by the two-order polynomial in numerical implementation.

We demonstrate the distance regularization effect of three distance regularized methods, DRLSE2, GRLSE, and our method DRLSE-E by simulating the diffusion mechanism with an initial binary step function on a 100×100 grid, with the region being a rectangle (see Fig. 2(a)). The effect of the distance regularization with the potentials can be seen from the following numerical simulation of the diffusion, as shown in Fig. 2(b)-(d), from where we can find three methods smooth the magnitude of gradient in the vicinity of the zero LS, however, only the double-well DRLSE2 and DRLSE-E preserve the characteristic of SDF and reduce the fluctuation of LS far away from zero LS. GRLSE smoothes the LS function on the whole domain with the failure of preserving the characteristic of SDF.

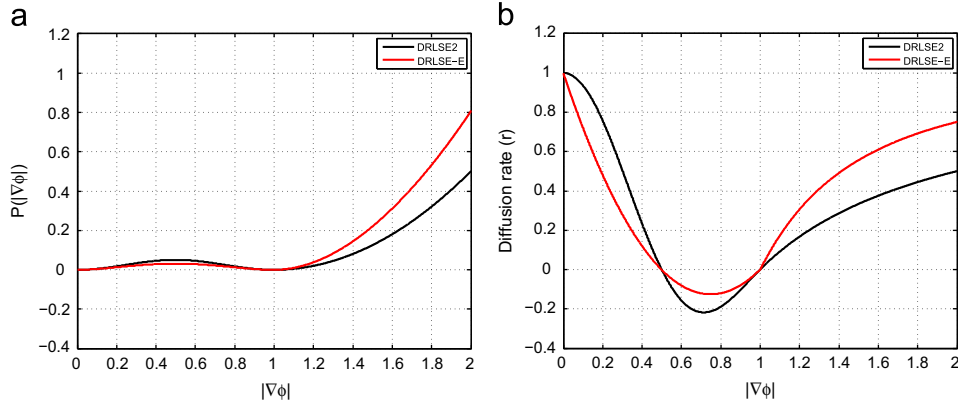


Fig. 1. Double-well potentials (a) and corresponding diffusion rates (b) of DRLSE2 and our DRLSE-E. (For interpretation of the references to color in this figure caption, the reader is referred to the web version of this paper.)

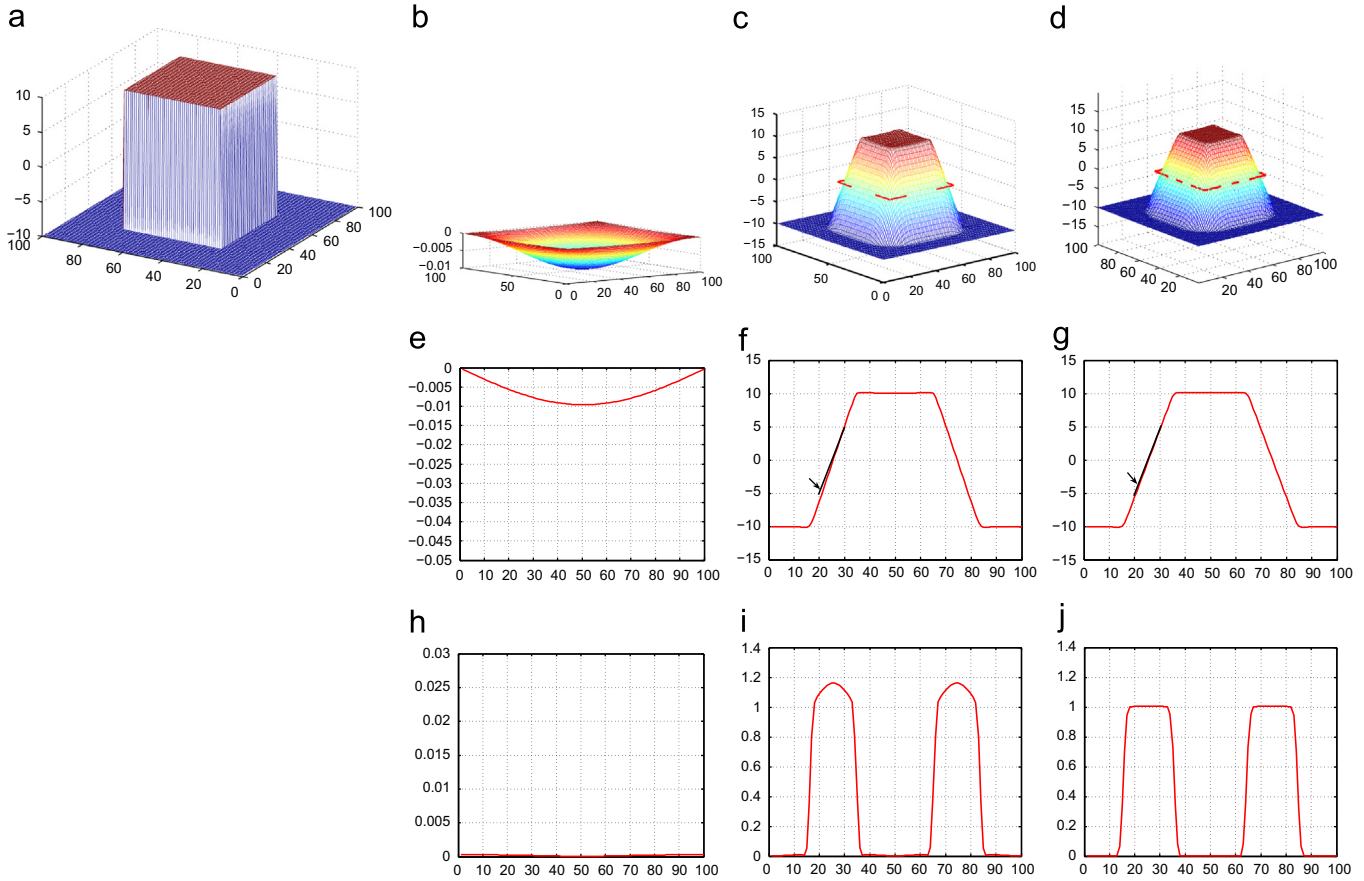


Fig. 2. Distance regularization effect on binary step function with the potentials of DRLSE2, GRLSE and DRLSE-E. (a) Initial LSF ϕ_0 ; (b)–(d) final LSFs of three methods; (e)–(g) cross sections on the LSFs of three methods; (h)–(j) cross sections of $|\nabla\phi|$ for the final function ϕ . (For interpretation of the references to color in this figure caption, the reader is referred to the web version of this paper.)

To visualize the regularization process of the diffusion in three methods, we plot the cross sections of $\phi(x, y), y = 50$ and $|\nabla\phi|$ on the second and third rows in Fig. 2. According to the basic idea of DRLSE2, the gradient of the LSF should approach to 1 as much as possible for capturing accurate zero LS contour, therefore, our DRLSE-E obtains more reasonable results than DRLSE2 in Fig. 2(f), (g), while the zero LS has disappeared by GRLSE2 in Fig. 2(e). From Fig. 2(h)–(j), we can find that DRLSE-E still preserves the characteristic of SDF, i.e. $|\nabla\phi| = 1$, in comparison to $|\nabla\phi| > 1$ in DRLSE2, and $|\nabla\phi| \rightarrow 0$ in GRLSE.

4. Implementation

4.1. DRLSE-E for image segmentation

The general DRLSE-E formulation in Eq. (21) can be incorporated in various applications with different definitions of the external energy. E.g.

$$\mathcal{E}(\phi) = \mu \mathcal{R}_P(\phi) + \mathcal{E}_{ext}(\phi), \quad (25)$$

where $\mathcal{R}_P(\phi)$ is the level set regularization term defined above, and $\mathcal{E}_{ext}(\phi)$ is the external energy that depends upon the data of interest. $\mu > 0$ is a constant. For image segmentation applications, a variety of image information can be employed to define the external energy. Typically, the edge-based model [15] defines the external energy functional as

$$\mathcal{E}_{ext}^{\text{GAC}}(\phi) = \lambda \mathcal{L}_g(\phi) + \alpha \mathcal{A}_g(\phi), \quad (26)$$

where a typical edge stopping function (ESF) g of an image I on a domain Ω is defined as $g = 1/(1 + |\nabla G_\sigma * I|^2)$; G_σ the Gaussian filter

with a standard deviation σ ; $\lambda > 0$ the coefficient of the length term $\mathcal{L}_g(\phi) = \int_{\Omega} g \delta(\phi) |\nabla\phi| d\mathbf{x}$ that computes the line integral of the function along the zero level contour of ϕ . $\mathcal{L}_g(\phi)$ reaches to its minimum when the zero LS is located at the object boundaries. $\alpha \in \mathbb{R}$ is the coefficient of the area term $\mathcal{A}_g(\phi) = \int_{\Omega} g H(-\phi) d\mathbf{x}$ that computes the weighted area of the region $\{\mathbf{x} | \phi(\mathbf{x}) < 0\}$. $\mathcal{A}_g(\phi)$ is introduced to speed up the motion of the zero level contour during the evolution, which is necessary when the initial contour is placed far away from the desired object boundaries. The sign of α is associated with the initial contour ϕ_0 , e.g., if ϕ_0 is placed outside the object, α should be positive and vice versa. Then the energy functional is approximated by

$$\mathcal{E}(\phi) = \mu \int_{\Omega} P(|\nabla\phi|) d\mathbf{x} + \lambda \int_{\Omega} g \delta(\phi) |\nabla\phi| d\mathbf{x} + \alpha \int_{\Omega} g H(-\phi) d\mathbf{x} \quad (27)$$

In calculus of variations, this energy functional can be minimized by solving the following gradient flow:

$$\frac{\partial \phi}{\partial t} = \mu \operatorname{div}(r \nabla \phi) + \delta(\phi) \left[\lambda \operatorname{div}\left(g \frac{\nabla \phi}{|\nabla \phi|}\right) + \alpha g \right], \quad (28)$$

where r is the diffusion rate in Eq. (23).

On the other hand, the region-based (or CV) model [25] defines the energy functional as

$$\begin{aligned} \mathcal{E}_{ext}^{\text{CV}}(c_1, c_2, C) = & \lambda \mathcal{L}_g(\phi) + \lambda_1 \int_{\text{inside}(C)} |I(x) - c_1|^2 d\mathbf{x} \\ & + \lambda_2 \int_{\text{outside}(C)} |I(x) - c_2|^2 d\mathbf{x} \end{aligned} \quad (29)$$

where $c_1(\phi) = \int_{\Omega} I(x)H(\phi) dx / \int_{\Omega} H(\phi) dx$, $c_2(\phi) = \int_{\Omega} I(x)(1-H(\phi)) dx / \int_{\Omega}(1-H(\phi)) dx$. In calculus of variations, this energy functional can be minimized by solving the following gradient flow:

$$\frac{\partial \phi}{\partial t} = \mu \operatorname{div}(r \nabla \phi) + \delta(\phi) \left[\lambda \operatorname{div}\left(\frac{\nabla \phi}{|\nabla \phi|}\right) - \lambda_1(I(x) - c_1)^2 + \lambda_2(I(x) - c_2)^2 \right] \quad (30)$$

4.2. Numerical implementation

In edge-based models, the Heaviside and Dirac functions $H(\phi)$, $\delta(\phi)$ are usually approximated by the following smooth functions:

$$H_{1,\epsilon}(x) = \begin{cases} \frac{1}{2} \left(1 + \frac{x}{\epsilon} + \frac{1}{\pi} \sin\left(\frac{\pi x}{\epsilon}\right) \right); & |x| \leq \epsilon \\ 1; & x > \epsilon \\ 0; & x < -\epsilon \end{cases} \quad (31)$$

$$\delta_{1,\epsilon}(x) = \begin{cases} \frac{1}{2\epsilon} \left[1 + \cos\left(\frac{\pi x}{\epsilon}\right) \right]; & |x| \leq \epsilon \\ 0; & |x| > \epsilon \end{cases} \quad (32)$$

The support of $\delta_{1,\epsilon}(x)$ is restricted into a neighborhood of zero LS so that the LSE can only act locally. In contrast, the region-based models usually employ a flatter function as

$$H_{2,\epsilon}(x) = \begin{cases} \frac{1}{2} \left(1 + \frac{2}{\pi} \arctan\left(\frac{x}{\epsilon}\right) \right); & |x| \leq \epsilon \\ 1; & x > \epsilon \\ 0; & x < -\epsilon \end{cases} \quad (33)$$

$$\delta_{2,\epsilon}(x) = \frac{1}{\pi} \cdot \frac{\epsilon}{\epsilon^2 + x^2}; x \in \mathbb{R} \quad (34)$$

The $\delta_{2,\epsilon}(x)$ acts on all level curves, and hence new contours can appear spontaneously, which makes it tend to yield a global minimum [25,34]. The parameter ϵ is usually settled as 1.5.

Incorporating with these approximations, we briefly present the numerical implementation to solve the evolutions in Eqs. (28), (30) via a simple, explicit finite difference scheme rather than a complex upwind scheme that is commonly used in conventional level set formulation. We consider the 2D case with a time-dependent level set function $\phi(x, y, t)$. The spatial derivatives $\partial\phi/\partial x$ and $\partial\phi/\partial y$ in our model are approximated by the central difference, and the temporal partial derivative $\partial\phi/\partial t$ is discretized as the forward difference. Let Δt be the time step, Δh the space step, $(x_i, y_i) = (i\Delta h, j\Delta h)$ the grid points, and $\phi_{ij}^n = \phi(x_i, y_i, n\Delta t)$ be an approximation of $\phi(x, y, t)$ with $n \geq 0$, $\phi^0 = \phi_0$, the accurate and efficient central differences are $d\phi_{x,y}/dx = (\phi_{i+1,j} - \phi_{i-1,j})/2\Delta h$; $d\phi_{x,y}/dy = (\phi_{i,j+1} - \phi_{i,j-1})/2\Delta h$. Set $k=0$, and start with initial level set function ϕ_{ij}^0 , the evolving process can be approached by $\phi_{ij}^{k+1} = \phi_{ij}^k + \Delta t L(\phi_{ij}^k)$, where $L(\phi_{ij}^k)$ is the right-hand of Eqs. (28), (30). Given spacial step $\Delta h = 1$, Δt for this finite difference scheme must satisfy the Courant–Friedrichs–Lowy (CFL) condition $\mu\Delta t < 0.25$. Similar to the reason pointed out by Li et al. [32,22], the added level set regularization term and the corresponding numerical scheme in our model is stable without the need for re-initialization.

In summary, the main steps of the algorithm are as follows.

Step 1 Initialize the level set function ϕ to a binary function ϕ_0 .

Step 2 Update the LSF.

Step 3 Check whether the evolution has stationary. If either the zero crossing points stop varying for consecutive iterations or exceed a prescribed maximum number of iterations, stop the iteration, otherwise, go to Step 2.

5. Experimental results

In this section, we evaluate and compare the proposed DRLSE-E model with typical active contour models, including GAC, CV [25], DRLSE1 [32], DRLSE2 [22], constrained DRLSE (DRLSE-C) [27], GRLSE [33], as well as RD [34]. In our experiments, the same initial contours are settled in the compared methods. The default setting of the parameters is chosen as for DRLSE, GRLSE, RD, and DRLSE-E, $c_0 = 2$, $\epsilon = 1.5$, $\Delta t = 1.0$, $\mu = 0.2$, $\lambda = 5.0$, $\alpha = 3.0$. All the experiments were conducted in Matlab 2009Ra platform on a Lenovo ThinkPad(R) notebook computer with Intel(R) i5 2.53 GHz CPU and 2G RAM.

We firstly apply DRLSE-E to edge-based variational level set models and secondly combine it with CV model in comparison with related methods. Thirdly, we quantitatively compare DRLSE-E with DRLSE-based methods for the edge-based and CV-based variational level set model. Finally, we report DRLSE-E's performance for real image segmentation.

5.1. Experiments with edge-based LSM

The DRLSE-E model is firstly used to segment a publicly available synthetic image with size 84×84 in Fig. 3(a) which is typical example of image with piecewise-constant intensities. Although small noise exists, the intensity values of the background and the object are remarkably different. The initial contour is a binary step function marked as blue rectangles in Fig. 3(b)–(f). The evolving processes (in other words, the convergent speeds) are marked using green curves to show the intermediate zero LSs with iteration interval 50. The parameter μ in GRLSE is 25, as suggested in [33]. The segmentation results are marked with red curves and the final LSs of each method are plotted in Fig. 3(g)–(k). From these we can find that all methods can converge to the right objects. Intuitively, GRLSE evolves very quick while RD evolves slower than other methods. Three distance regularized methods evolve similar and our DRLSE-E is faster than DRLSE1 and DRLSE2. DRLSE1 creates unnecessary peaks and valleys in the regions away from zero LS for confining it to the SDF locally. The similar final LSs of DRLSE2 and DRLSE-E preserve the property of both $|\nabla\phi|=1$ and $|\nabla\phi|=0$ in different regions, slightly better than that of GRLSE. They all are smoother than those of DRLSE1 and RD methods.

To further test the performance of our DRLSE-E on segmenting complex objects in inhomogeneous background, we conducted another experiment on a widely used synthetic image with sizes 79×75 in Fig. 4(a). It is a typical testing image with varying intensities in objects and backgrounds. The key characteristics of these methods and our experimental scheme are similar to the first one. The intermediate zero LSs of the compared methods are plotted in Fig. 4(b)–(f). The segmentation results are marked with red curves for each method. The final LSs of each method are plotted in Fig. 4(g)–(k). The final LSs clearly distinct the flat regions in objects as well as background. In other words, the property of $|\nabla\phi|=0$ is preserved in these regions. On the other hand, the binary step-like signed distance bands are narrow in the clear or obscure edges of the objects, which means the property of $|\nabla\phi|=1$ is properly preserved. This result is in accordance to the discussion in Fig. 2, where the magnitude of $\nabla\phi$ is closer to the right value than other methods, ensuring the performance of exacter segmentation in real-world images.

These evolving iso-contours and the final LSs indicate that the proposed DRLSE-E are more robust to segment the inhomogeneous objects in inhomogeneous background under a limited iteration. Furthermore, the three distance regularized methods can capture the right contour of the complex objects in this case, contrarily, GRLSE fails to extract the star-like object due to its global mean estimation. RD produces remarkable boundary leakage.

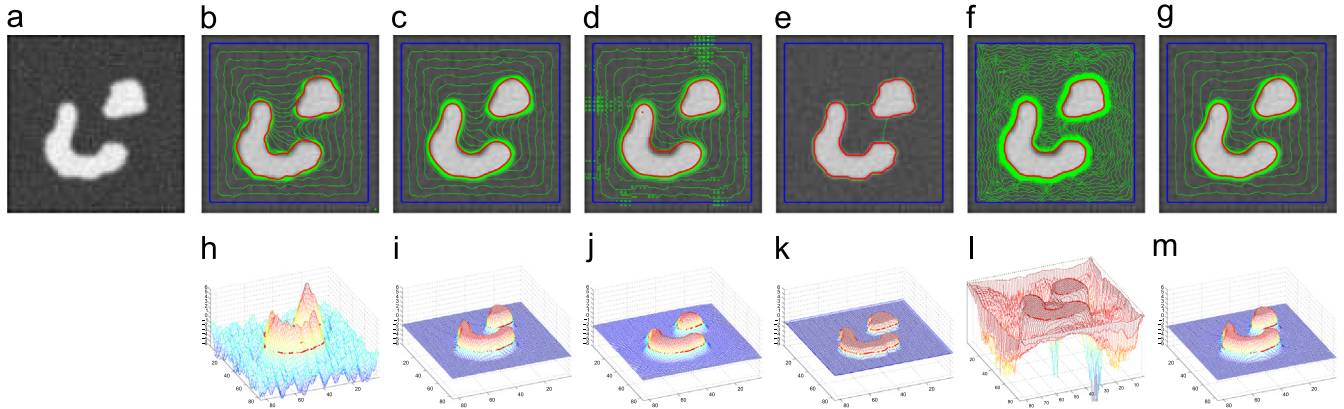


Fig. 3. Evolution process and 3D view of final LS by edge-based model on a synthetic image (a) with homogeneous background by DRLSE1 (b), (h); DRLSE2 (c), (i); DRLSE-C (d), (j); GRLSE (e), (k); RD (f), (l) and our DRLSE-E methods (g), (m). The initial and final zero LSs are marked by blue and red curves respectively. (For interpretation of the references to color in this figure caption, the reader is referred to the web version of this paper.)

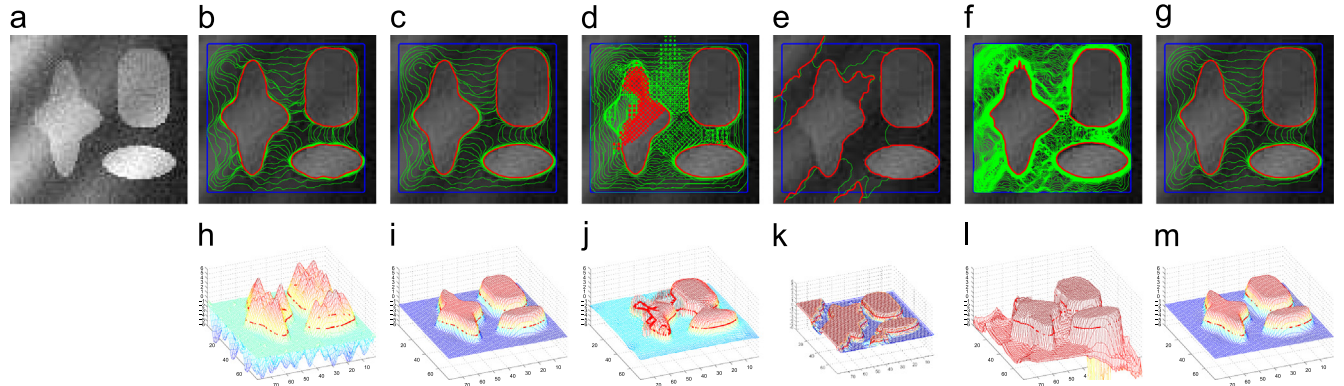


Fig. 4. Evolution process and 3D view of final LS by edge-based model on a synthetic image (a) with both inhomogeneous objects and background by DRLSE1 (b), (h); DRLSE2 (c), (i); DRLSE-C (d), (j); GRLSE (e), (k); RD (f), (l) and our DRLSE-E methods (g), (m). The initial and final zero LSs are marked by blue and red curves respectively. (For interpretation of the references to color in this figure caption, the reader is referred to the web version of this paper.)

Fig. 5 shows the results of the proposed DRLSE-E on five natural and medical images: a life image with two high contrast objects in dark background (336×335 size), a tool image with line and corner structure (335×333 size), a MR image of a human bladder (436×260 size), a CT image with a tumor (the dark area) in human liver (321×336 size), and a star-like image in noisy background with similar intensities (362×331 size). For this experiment, we used the narrow-band implementation of the DRLSE-E model by a C program in Mex format, with the smallest parameter in the narrow-band construction. The CPU times were recorded for the five images by running the program ten times repeatedly to evaluate the real-time capability. We tested the robustness of the model under different initialization LSs, as shown in the images on the first column in **Fig. 5**, these initialized LSs vary from types of covering all the objects to types of lying in the objects. The binary functions are used to initialize the LSFs by marking the blue curves. It is found that the DRLSE-E method yields desirable segmentation results without boundary leakage, and the final LSFs are piecewise constant.

5.2. Experiments with region-based LSM

We combined our DRLSE-E method with the CV model to segment a publicly natural image with size 320×240 in **Fig. 6(a)**, which is typical example of image with object in inhomogeneous background. There is slight noise in the image. The initial contour

is a binary step function marked as blue rectangles in **Fig. 3(b)–(f)**. The evolving processes (in other words, the convergent speeds) are marked using green curves to show the intermediate zero LSs with iteration interval 50. The segmental results are marked with red curves and the final LSs of each method are plotted in **Fig. 3(g)–(k)**. From these we can find that all methods can converge to the right objects. Intuitively, RD and our method obtain better results than other methods. Although CV assumes that the image intensity is piecewise constant, it produces unsmooth mesh when lack of re-initialization. Three distance regularized methods evolve similar and our DRLSE-E is better than DRLSE1 and DRLSE2.

In order to demonstrate that our DRLSE-E with CV model can reach the global minimum while being robust to level set initializations, we apply it to a noisy synthetic image with different level set initializations, as shown in **Fig. 7**, the zero contours are set outside the objects, inside one object, cross some objects, or even around all the objects. Although these initializations vary, the final contours are almost the same, which validates that our method can robustly evolve to the global minimum of the energy functional, leading a good global segmentation. It is noticed that these segmentation curves are not identical, mainly due to that practically $|\nabla\phi| \approx 1$ or $|\nabla\phi| \approx 0$ in the presence of the numerical implementation in digital image.

We further tested DRLSE-E with CV-based model on four real images. As shown in **Fig. 8**, the object contours can be accurately

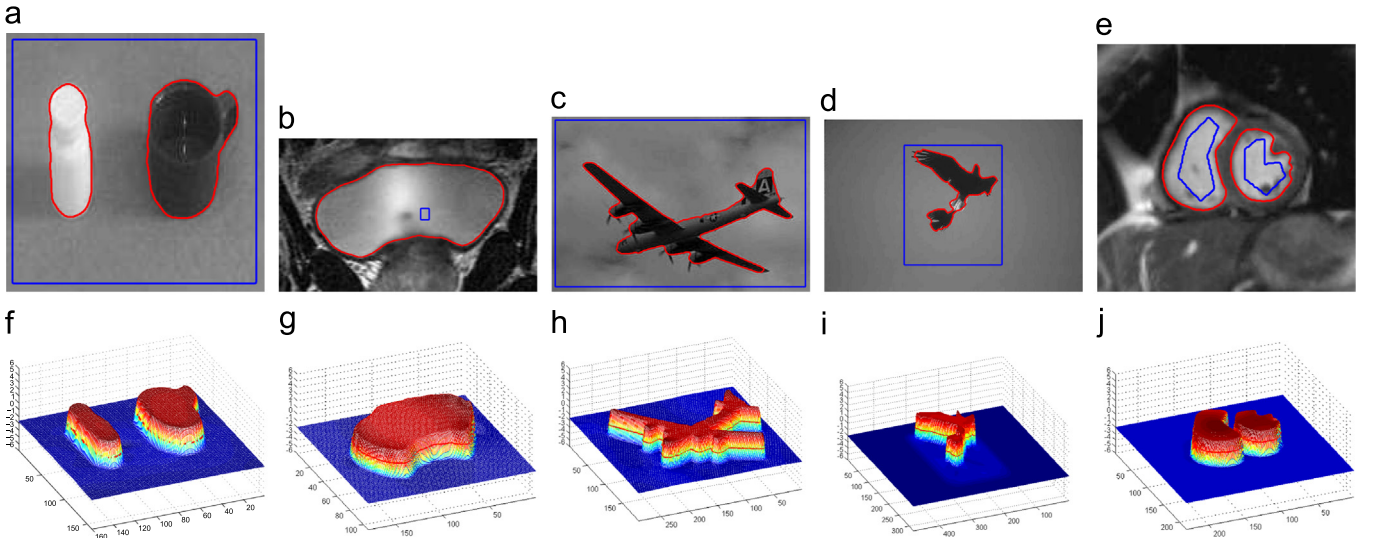


Fig. 5. Results of DRLSE-E with edge-based model for five real images. Different initial LSs and final zero iso-contours are marked as blue and rectangles respectively. The average CPU times are 0.47, 0.29, 0.34, 0.26, and 0.37 s consumed. (For interpretation of the references to color in this figure caption, the reader is referred to the web version of this paper.)

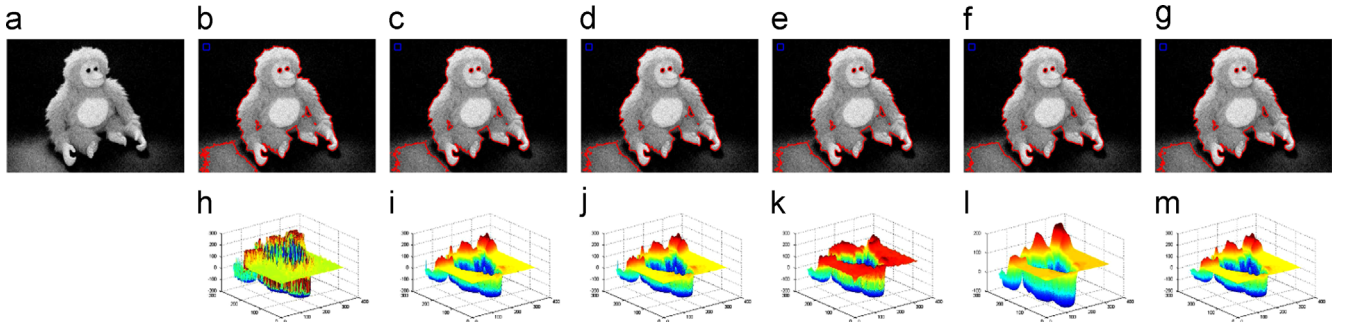


Fig. 6. Evolution process and 3D view of final LS by region-based model on a monkey image (a) with inhomogeneous background by CV (b), (h); DRLSE1 (c), (i); DRLSE2 (d), (j); DRLSE-C (e), (k); RD (f), (l) and our DRLSE-E methods (g), (m). The initial and final zero LSs are remarked by blue and red curves respectively. (For interpretation of the references to color in this figure caption, the reader is referred to the web version of this paper.)

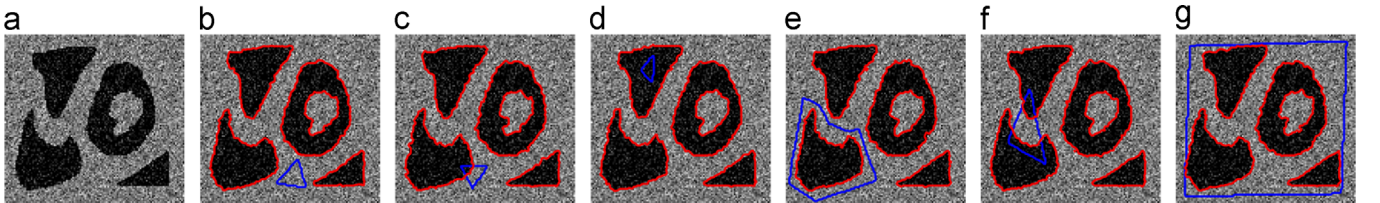


Fig. 7. Robustness of our DRLSE-E method with CV model in different level set initializations. The parameters for all images are $\Delta t = 0.1$, $\lambda_1 = \lambda_2 = 1$, $\mu = 0.2/\Delta t$. Different initial LSs and final zero iso-contours are marked as blue and red curves respectively. (For interpretation of the references to color in this figure caption, the reader is referred to the web version of this paper.)

extracted from complex backgrounds. For the hand image and the plane image, the LSE is easy to fall into local minima due to the backgrounds. However, based on the competing components discussed in Section 3.2, DRLSE-E is still able to obtain the global minimum. The final segmental results are robust to initialization: we can use the simple rectangle initialization in different position to yield good segmentation results for these images. This demonstrates that the parameters are robust to different images by our method.

5.3. Quantitative experiments on synthetic images

To quantitatively evaluate the performance of DRLSE-E combining the edge-based and region-based models, we use it to segment six synthetic images of known true object. As suggested

in [34], we employ the Jaccard similarity (JS) index to quantitatively evaluate the segmentation performance of these methods. This JS index is the ratio between intersectional area of S_1 and S_2 and their united area, i.e.

$$J(S_1, S_2) = \frac{\text{area}(S_1 \cap S_2)}{\text{area}(S_1 \cup S_2)} \quad (35)$$

The closer the J is to 1, the more similar S_1 is to S_2 . In our experiments, S_1 is the segmented region by the six compared methods, and S_2 is the ground truth.

The compared methods include GAC, CV, DRLSE1, DRLSE2, GRLSE, and RD methods. Their segmentation accuracies and time consumptions are report in Figs. 9 and 10 respectively. In Figs. 9(a)–(c) and 10(a)–(c), each with high curvature objects, sharp edges whose boundary is known and used as the ground truth. The employed LS

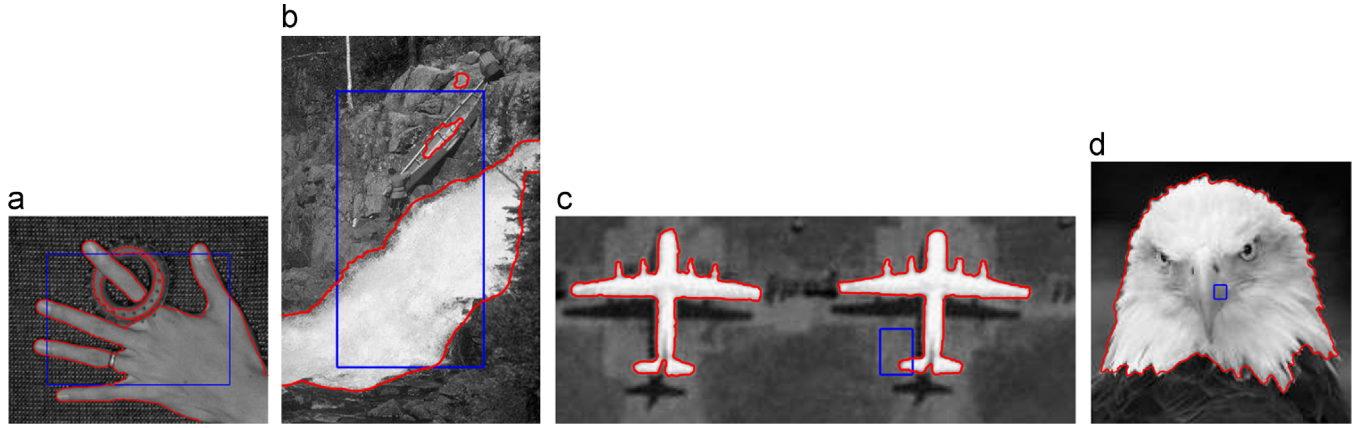


Fig. 8. Results of our DRLSE-E method with CV model on four real images. Different initial LSs and final zero iso-contours are marked as blue and rectangles respectively. (For interpretation of the references to color in this figure caption, the reader is referred to the web version of this paper.)

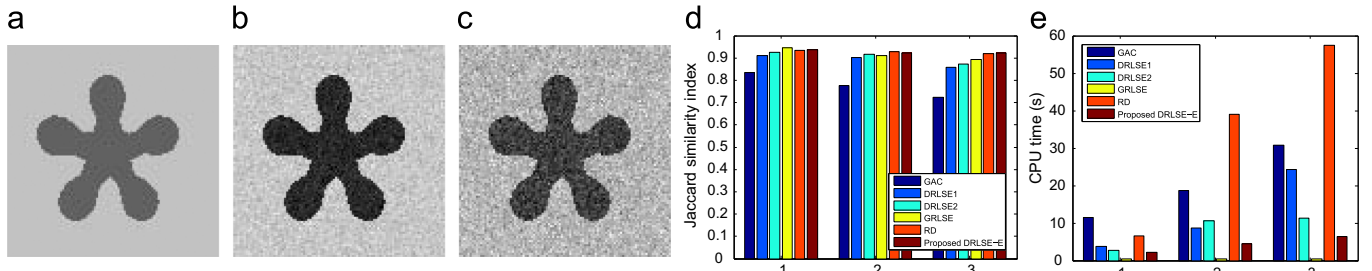


Fig. 9. Quantitative comparisons among six compared methods for edge-based models. (a) Clean image; (b) noisy image (Gaussian noise with zero mean and standard deviation $\sigma=0.001$); (c) noisy image (Gaussian noise with zero mean and standard deviation $\sigma=0.005$); (d) the Jaccard similarity index J ; (e) the CPU times for different methods. $\sigma=1.0$ in Gaussian smoothing for edge stop function g . For edge-based variational models, we set $\Delta t=1$, $\lambda=5$, $\alpha=3$, $\epsilon=1.5$, for the RD model, we set $\Delta t_1=0.1$, $\Delta t_2=0.001$, $F=0.5$, and for the GAC model, we set $\Delta t=0.1$, $F=3$, and re-initialization interval as 50 for all the three images.

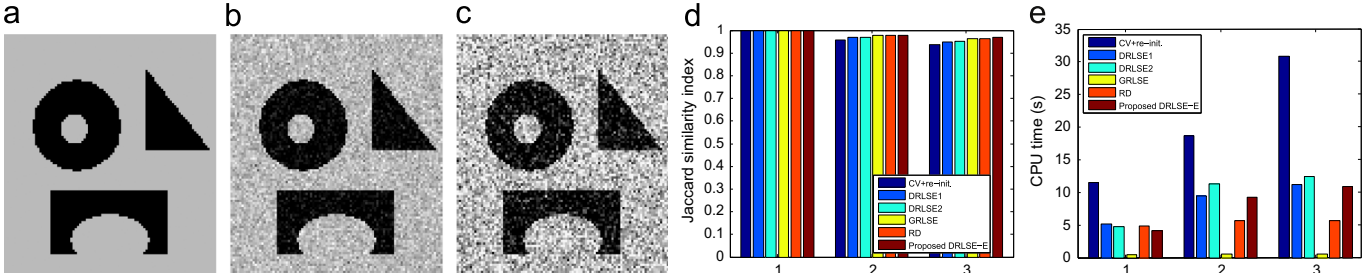


Fig. 10. Quantitative comparisons among five methods for region-based models. (a) Clean image; (b) noisy image (Gaussian noise with zero mean and standard deviation $\sigma=0.01$); (c) noisy image (Gaussian noise with zero mean and standard deviation $\sigma=0.05$); (d) the Jaccard similarity index J ; (e) the CPU times for different methods. We set $\Delta t=1$, $\lambda_1=\lambda_2=1$, $\mu=0.1 \times 255^2$. For RD we set $\Delta t_1=0.1$, $\Delta t_2=0.001$. For CV with re-initialization method, the re-initialization interval is 50. (For interpretation of the references to color in this figure caption, the reader is referred to the web version of this paper.)

was GAC-based and CV-based variational models. We used the same initial contour for all models except GAC model, which needed a standard SDF that is re-initialized in every 10 iteration interval. When the difference of two neighboring contours of the zero LSs is less than three pixels, the evolution stopped. For GRLSE, we settled a fixed iteration number since its zero LS will disappear. Due to the randomness of added Gaussian noise, the program was conducted 50 times and then the mean of J was estimated. The CPU times were recorded during these 50 repeating and the average time consumption was calculated as indices for measuring the efficiency of each method. The compared methods were programmed just based the public protocol codes in [22,32–34] and not algorithmic optimization or programming technique was taken into consideration, nor narrow band constriction or other skills was incorporated into the compared methods. The parameters in these methods were settled as same as possible for fair comparison, except the iteration number and the exclusive

parameters of each method. It should be noted that the larger Δt_1 , Δt_2 , F can speed up the evolution of LSs in the RD model, but easily make boundary leakage or zero LS disappear, so we put the segment accuracy as the first place in selection of these parameters.

The JS indices and the average CPU time consumption seconds by applying the six competing methods are reported in Figs. 9(d), (e) and 10(d), (e), from where we can see:

- (1) The models free of re-initialization can achieve better segmenting accuracy than GAC and CV with standard re-initialization step. This means that the re-initialization step does not thoroughly preserve the signed distance property of LS and therefore decreases the segmentation accuracy.
- (2) Among the models free of re-initialization, the proposed DRLSE-E achieves competitive accuracy. Its JS index is slightly higher than other models and remarkable higher than DRLSE1



Fig. 11. Segmentation using the proposed DRLSE-E and 3D reconstruction of white matter on the second Chinese Visible Human (CVH02) data set. (a)–(e) and (k)–(o) are ROI sub-images from the original 3872×2048 size images, while (f)–(j) and (p)–(t) are corresponding segmental results, all with the same size of 852×974 . The interval of two nearby images is 10. (u) is the 3D reconstruction software platform developed by the first author and (v) is the final 3D reconstruction result. The parameters were adjusted according to the components in the images and the context constrains, typically $\Delta t = 0.1\sim 1$, $\alpha = 3$, $\lambda = 1$ in the experiments. The CPU time is less than 10 min for the whole segmentation task. (For interpretation of the references to color in this figure caption, the reader is referred to the web version of this paper.)

model. This fact is interpretable since DRLSE-E adaptively preserves $|\nabla\phi|=1$ or $|\nabla\phi|=0$ in different regions while DRLSE1 only tries to preserve $|\nabla\phi|=1$ in LS evolution. DRLSE-E is comparable to DRLSE2 because it can achieve faster diffusion rates than DRLSE2 in same regions. The GRLSE and RD models can achieve remarkable high JS index in clean image, however, the accuracy of GRLSE model decrease faster than RD model when segmenting noisy images. This fact is due to GRLSE utilizes gray mean of object and background, which is more distinctive in clean image than in noisy images. Contrarily, DRLSE-E shows stable accuracy on these images. This means that the appreciate diffusion rates during LS evolution are advisable for anti-noisy image segmentation.

- (3) The evolving speed of DRLSE-E is competitive in all methods except GRLSE. GRLSE can finish tasks in one second, remarkably consuming less CPU time than other methods, however, the evolution of GRLSE theoretically cannot converge to the objects eventually and how to stop the iteration is difficult in practice, as we treated it in an ad hoc manner in the experiments. On the other hand, although the segmenting accuracy of RD model is very close to our model, its evolving speed seems varying, restricting its application in segmenting real image with larger size. When the noise is strengthened, the time consumption of our model is increased, but still faster than the two DRLSE models due to its characteristics of diffusion rates. This quantitative experiment demonstrates the competence of DRLSE-E in the viewpoint of overall segmentation accuracy, efficiency, and robust anti-noise performance.

5.4. Experiments on medical serial images segmentation

In this subsection, we report results of DRLSE-E in C++ language version for segmenting the white matter of the second Chinese visible human (CVH02) serial images. The human specimen of this data set is a 22 years old, 162 cm height, 52 kg weight female body from an Asian population. This CVH02 data set is characterized as high-quality image data integrity through the improvements of large milling machine table to avoid data loss caused by fragmenting the body before cryomacrotoming, and of the -25°C temperature room to prevent small structures (including tooth, concha nasalis and articular cartilage) from falling off the milling surface [42]. The transverse section images were captured by an external computer using a Canon EOS-D60 (R) digital camera (resolution 3072×2048 correspond to approximate $170 \mu\text{m}$ pixel size), and the milling interval varies from 0.1 mm to 1 mm according to different parts and produces 3640 slices. This data set is so huge (131.04 GB) that brings new challenge to existing segmentation algorithms.

We chose brain white matter as the object to be segmented because of its importance in various medical applications and the whole data acquisition (e.g. the 0.1–0.25 mm interval for the head while 0.5 mm for the legs). According to this, firstly we selected the ROI sub-image of 852×974 size from the 1096th to 1495th images, as the samples of 10 slice interval shown in Fig. 11(a)–(e), (k)–(o) with RGB color model, then we transformed them to the HSV color space and used the hue component images for segmentation, further we adjusted the experimental parameters according to real sections of the white matter and the context constrains among the image slices, at last we conducted the DRLSE-E based segmentation and 3D reconstruction. The examples of segmentation result are reported in Fig. 11(f)–(j), (p)–(t). These images are taken from our SeadriftMedical software platform developed by the first author using Microsoft VS studio 2010(R). As shown in Fig. 11(u), three orthogonal or non-orthogonal images can be observed from this software. Furthermore, the 3D reconstruction result according to the 2D segment images is shown in Fig. 11(v).

From the digitized ROI images we can find that although the brain white matter can be distinguished from the brain gray matter by human expert, the edge largely varies from clear to obscure, moreover, the brain white matter is heavily inhomogeneous and un-connected in z direction. It was estimated that an expert had to take forty minutes per image, one month for all images to extract this object by manual segmentation, so this task had to be interrupted. Such difficulties were overcome by the proposed DRLSE-E under the software, only taking ten minutes with an acceptable visual effect because DRLSE-E allows using relatively large time steps to significantly reduce iteration numbers and computation time. The segmentation result was applicable to estimate the brain white matter area and voltage, also was advisable by the medical researchers in the fields of brain functional imaging. To the best of our knowledge, it is the first 3D data result of high-resolution brain white matter on CVH using computer-aided segmentation technique. Considering the characteristic of this application, our algorithm can be easily applied to other similar real-world segmentation tasks.

6. Conclusions

We have presented an enhanced distance regularized LS method (DRLSE-E) completely free of the re-initialization. DRLSE-E has an intrinsic capability of maintaining regularity of LSF, particularly the desirable signed distance property in a vicinity of the zero LS and the flat property out at this vicinity, which ensures accurate computation and stable LS evolution. As an extension of the recent appeared distance regularized, Gaussian regularized, reaction-diffusion based LS methods (DRLSE, GRLSE, and RD), DRLSE-E shares the characteristics of DRLSE, such as simpler and more efficient numerical scheme in implementation, more flexible and efficient initialization than conventional LS methods. Moreover, DRLSE-E has the advantage of faster evolving speed and more numerical accuracy than DRLSE because its forward-backward diffusion rate is more reasonable during the evolving procedure. The image segmentation experiments show its competence in comparison to five related methods. Considering DRLSE-E is general, it can be easily incorporated into the various existing LS models for image segmentation, filtering, and other tasks. We will explore its utility in more applications in the future.

Acknowledgments

This work was partially supported by the Chinese National Science Foundation (NSFC 60903142, 61190122), the China Postdoctoral Science Foundation (2013T60841, 2012M521677, Xm201306), and the Natural Science Foundation of CQ-CSTC (CSTC2009BB3192, cstc2011jjA40024), the Sci & Tech Research Project of Chongqing Municipal Education Commission (KJ120601), and Fundamental Research Funds for the Central Universities (106112013CDJZR120001). The authors gratefully acknowledge the helpful comments and suggestions of the reviewers, which have improved the presentation.

References

- [1] M. Kass, A.P. Witkin, D. Terzopoulos, Snakes: active contour models, *Int. J. Comput. Vis.* 1 (4) (1988) 321–331.
- [2] S.C. Zhu, A.L. Yuille, Region competition: unifying snakes, region growing, and Bayes/MDL for multiband image segmentation, *IEEE Trans. Pattern Anal. Mach. Intell.* 18 (9) (1996) 884–900.
- [3] Y. Wang, D. Tao, X. Gao, X. Li, B. Wang, Mammographic mass segmentation: embedding multiple features in vector-valued level set in ambiguous regions, *Pattern Recognit.* 44 (9) (2011) 1903–1915.
- [4] B. Wang, X. Gao, D. Tao, X. Li, A unified tensor level set for image segmentation, *IEEE Trans. Syst. Man Cybern. Part B* 40 (3) (2010) 857–867.

- [5] R. Tsai, S. Osher, Level set methods and their applications in image science, *Commun. Math. Sci.* 1 (4) (2003) 623–656.
- [6] S. Balla-Arabe, X. Gao, Image multi-thresholding by combining the lattice Boltzmann model and a localized level set algorithm, *Neurocomputing* 93 (2012) 106–114.
- [7] D. Mumford, J. Shah, Optimal approximations by piecewise smooth functions and associated variational problems, *Commun. Pure Appl. Math.* 42 (1989) 577–685.
- [8] C.Y. Xu, J.L. Prince, Snakes, shapes, and gradient vector flow, *IEEE Trans. Image Process.* 7 (3) (1998) 359–369.
- [9] S. Osher, J.A. Sethian, Fronts propagating with curvature dependent speed: algorithms based on Hamilton-Jacobi formulations, *J. Comput. Phys.* 79 (1988) 12–49.
- [10] S. Osher, R.P. Fedkiw, *The Level Set Method and Dynamic Implicit Surfaces*, Springer-Verlag, New York, 2002.
- [11] X. Gao, B. Wang, D. Tao, X. Li, A relay level set method for automatic image segmentation, *IEEE Trans. Syst. Man Cybern. Part B* 41 (2) (2011) 518–525.
- [12] S. Balla-Arabe, X. Gao, B. Wang, Gpu accelerated edge-region based level set evolution constrained by 2d gray-scale histogram, *IEEE Trans. Image Process.* 22 (7) (2013) 2688–2698.
- [13] S. Balla-Arabe, X. Gao, B. Wang, A fast and robust level set method for image segmentation using fuzzy clustering and lattice Boltzmann method, *IEEE Trans. Cybern.* 43 (3) (2013) 910–920.
- [14] R. Malladi, J.A. Sethian, B.C. Vemuri, Shape modeling with front propagation: a level set approach, *IEEE Trans. Pattern Anal. Mach. Intell.* 17 (2) (1995) 158–175.
- [15] V. Caselles, R. Kimmel, G. Sapiro, Geodesic active contours, *Int. J. Comput. Vis.* 22 (1) (1997) 61–79.
- [16] G. Barles, H.M. Soner, P.E. Souganidis, Front propagation and phase field theory, *SIAM J. Control Optim.* 31 (2) (1993) 439–469.
- [17] M. Sussman, P. Smereka, S. Osher, A level set approach for computing solutions to incompressible two-phase flow, *J. Comput. Phys.* 114 (1994) 146–159.
- [18] J.A. Sethian, *Level Set Methods and Fast Marching Methods*, Cambridge University Press, Cambridge, UK, 1999.
- [19] G. Russo, P. Smereka, A remark on computing distance functions, *J. Comput. Phys.* 163 (1) (2000) 51–67.
- [20] D. Peng, B. Merriman, S. Osher, H. Zhao, M. Kang, A PDE-based fast local level set method, *J. Comput. Phys.* 155 (1999) 410–438.
- [21] J. Gomes, O. Faugeras, Reconciling distance functions and level sets, *J. Vis. Commun. Image Represent.* 11 (2) (1999) 209–223.
- [22] C. Li, C. Xu, C. Gui, M.D. Fox, Distance regularized level set evolution and its application to image segmentation, *IEEE Trans. Image Process.* 19 (12) (2010) 3243–3254.
- [23] M. Nikolova, S. Esedoglu, T.F. Chan, Algorithms for finding global minimizers of image segmentation and denoising models, *SIAM J. Appl. Math.* 66 (5) (2006) 1632–1648.
- [24] X. Bresson, S. Esedoglu, P. Vandergheynst, J.-P. Thiran, S. Osher, Fast global minimization of the active contour/snake model, *J. Math. Imaging Vis.* 28 (2) (2007) 151–167.
- [25] T.F. Chan, L.A. Vese, Active contours without edges, *IEEE Trans. Image Process.* 10 (2) (2001) 266–277.
- [26] L.A. Vese, T.F. Chan, A multiphase level set framework for image segmentation using the Mumford and Shah model, *Int. J. Comput. Vis.* 50 (3) (2002) 271–293.
- [27] X. Xie, Active contouring based on gradient vector interaction and constrained level set diffusion, *IEEE Trans. Image Process.* 19 (1) (2010) 154–164.
- [28] X. Xie, M. Mirmehdii, Initialisation-free active contour segmentation, in: Proceedings of 20th International Conference on Pattern Recognition (ICPR 2010), Istanbul, Turkey, 23–26 August 2010, 2010, pp. 2318–2321.
- [29] X. Xie, M. Mirmehdii, Radial basis function based level set interpolation and evolution for deformable modelling, *Image Vis. Comput.* 29 (2–3) (2011) 167–177.
- [30] V. Estellers, D. Zosso, R. Lai, S. Osher, J.-P. Thiran, X. Bresson, Efficient algorithm for level set method preserving distance function, *IEEE Trans. Image Process.* 21 (12) (2012) 4722–4734.
- [31] T. Goldstein, S. Osher, The split Bregman method for L1-regularized problems, *SIAM J. Imaging Sci.* 2 (2) (2009) 323–343.
- [32] C. Li, C. Xu, C. Gui, M. D. Fox, Level set evolution without re-initialization: a new variational formulation, in: Proceedings of 2005 IEEE Computer Society Conference on Computer Vision and Pattern Recognition (CVPR 2005), 20–26 June 2005, San Diego, CA, USA, 2005, pp. 430–436.
- [33] K. Zhang, L. Zhang, H. Song, W. Zhou, Active contours with selective local or global segmentation: a new formulation and level set method, *Image Vis. Comput.* 28 (4) (2010) 668–676.
- [34] K. Zhang, L. Zhang, H. Song, D. Zhang, Reinitialization-free level set evolution via reaction diffusion, *IEEE Trans. Image Process.* 22 (1) (2013) 258–271.
- [35] B. Merriman, J.K. Bence, S.J. Osher, Motion of multiple junctions, a level set approach, *J. Comput. Phys.* 112 (2) (1994) 334–363.
- [36] S. Baldo, Minimal interface criterion for phase transitions in mixtures of Cahn–Hilliard fluids, *Ann. Inst. Henri Poincaré* 7 (1990) 67–90.
- [37] J.-J. Xu, H.-K. Zhao, An Eulerian formulation for solving partial differential equations along a moving interface, *J. Sci. Comput.* 19 (1–3) (2003) 573–594.
- [38] Y. Wang, C. He, Adaptive level set evolution starting with a constant function, *Appl. Math. Model.* 36 (7) (2012) 3217–3228.
- [39] M. Burger, S.J. Osher, A survey on level set methods for inverse problems and optimal design, *Eur. J. Appl. Math.* 16 (02) (2005) 263–301.
- [40] G. Gilboa, N.A. Sochen, Y.Y. Zeevi, Forward-and-backward diffusion processes for adaptive image enhancement and denoising, *IEEE Trans. Image Process.* 11 (7) (2002) 689–703.
- [41] M. Welk, G. Gilboa, J. Weickert, Theoretical foundations for discrete forward-and-backward diffusion filtering, in: X.-C. Tai, K. Mørken, M. Lysaker, K.-A. Lie (Eds.), *Proceedings of 2nd International Conference on Scale Space and Variational Methods in Computer Vision (SSVM 2009)*, Lecture Notes in Computer Science, vol. 5567, Voss, Norway, 2009, pp. 527–538.
- [42] S.-X. Zhang, P.-A. Heng, Z.-J. Liu, L.-W. Tan, M.-G. Qiu, Q.-Y. Li, R.-X. Liao, K. Li, G.-Y. Cui, Y.-L. Guo, X.-P. Yang, G.-J. Liu, J.-L. Shan, J.-J. Liu, W.-G. Zhang, X.-H. Chen, J.-H. Chen, J. Wang, W. Chen, M. Lu, J. You, X.-L. Pang, H. Xiao, Y.-M. Xie, J.-C.-Y. Cheng, The Chinese visible human (CVH) datasets incorporate technical and imaging advances on earlier digital humans, *J. Anat.* 204 (3) (2004) 165–173.



Xuchu Wang received his MSc and PhD degrees in mechanical engineering and its automation, instrument science and technology from Chongqing University (CQU), China, in 2002 and 2007, respectively. He then joined CQU in July 2007 and is currently an associate professor in the College of Optoelectronic Engineering and a research faculty in the Key Laboratory of Optoelectronic Technology and Systems of Ministry of Education. Since 2013, He is a CSC-sponsored visiting scholar in the Biomedical Research Imaging Center (BRIC) of the University of North Carolina at Chapel Hill (UNC). He received the “10 university-wide outstanding PhD dissertation award” and “10 university-wide distinguished high-level journal paper award” for his research work on image processing and biometrics. His research interests are medical image analysis, statistical pattern recognition, biometrics (mainly based on fingerprint and face), and practical PR/biometrics system development, where he had more than 20 peer-reviewed papers published.

Jinxiao Shan received his BSc degree in instrument science and technology from Jiangxi University of Science and Technology in June 2010. He was a postgraduate student in the College of Optoelectronic Engineering, Chongqing University. His research interest is medical image analysis.

Yanmin Niu received her BSc and MSc degrees in instrument science and technology from Chongqing University in 1997 and 2003, respectively. Currently she is an associate professor with the College of Computer and Information Science, Chongqing Normal University. Her research interests include medical image analysis, and machine learning, where she had more than 20 peer-reviewed papers published.

Liwen Tan received his Master degree in computer engineering from Third Military Medical University in June 2003. Currently he is a senior experimentalist in the Department of Anatomy, Third Military Medical University. His research interest is Chinese visible human research and medical image analysis, where he has more than 50 peer-reviewed papers published.

Shao-Xiang Zhang received his medical doctor degree from Third Military Medical University in June 1995. Currently he is a professor in the Department of Anatomy, Third Military Medical University. His research interest is Chinese visible human research and medical image analysis, where he has more than 100 peer-reviewed papers published.